A novel formula for predicting the ultimate compressive strength of the cylindrically curved plates

Do Kyun Kim [a,b,*], Andy Ming King Wong [c], Jinha Hwang [d], Shen Li [e], Nak-Kyun Cho [f,**]

[a] Department of Naval Architecture and Ocean Engineering, College of Engineering, Seoul National University, Seoul, Republic of Korea
[b] Research Institute of Marine Systems Engineering, Seoul National University, Seoul, Republic of Korea
[c] Department of Civil and Environmental Engineering, PETRONAS University of Technology, Seri Iskandar, Perak, Malaysia
[d] Department of Mechanical Engineering, Pukyong National University, Pusan, Republic of Korea
[e] Department of Naval Architecture, Ocean and Marine Engineering, University of Strathclyde, Glasgow, United Kingdom
[f] Department of Manufacturing Systems and Design Engineering, Seoul National University of Science and Technology (SeoulTech), Seoul, Republic of Korea

ARTICLE INFO

ABSTRACT

"The present study aims to develop an empirical formula to predict the ultimate compressive strength of unstiffened cylindrically curved plates. Drawing from an extensive analysis of 400 unique curved plate scenarios under longitudinal compression, we investigated critical parameters: the flank angle (denoted as θ), plate aspect ratio (denoted as a/b), and plate slenderness ratio (denoted as β). The ANSYS Nonlinear Finite Element Method (NLFEM) was employed to assess each scenario, considering the average level of initial imperfections (denoted as $0.1\beta^2 t$) and configurations of one-bay and one-span. It is important to note that the models were designed without accounting for the effects of residual stresses. The simulation data generated from this analysis served as the foundation for developing our empirical formula. The proposed formula strongly agreed with the numerical simulations and experimental test results. This research provides structural engineers with a reliable predictive tool, aiding in more accurate predictions of the ultimate limit state (ULS) of curved plates during early design phases.

1. Introduction

Thin-walled cylindrical shells are widely used as structural elements, such as oil and gas storage, offshore structures, cooling towers, wind towers and ship hulls. In general, cylindrically curved plates or cylindrically unstiffened panels, herein "curved plates", are extensively used in ship structures, such as chambered deck plating, side shell plating fore and aft, and bilge circle parts of ships. Therefore, it is essential to clarify the elastic and plastic stability of cylindrically curved plates under various loading conditions. Park et al. (2018) showed excellent pictures of the curved plates and stiffened panels in ultra-large container vessels, including the ship's stern and bilge strake parts.

The structural modelling and investigation of stiffened and unstiffened curved plates can fundamentally be treated as a part of the cylinder. From estimations made using cylinder models, it is known that curvature increases the buckling strength of a curved plate subjected to axial compression. Besides, the curvature is expected to increase the ultimate strength performance of the curved plate. On top of that, the curved plate is commonly used for modern design standards of economical vessels that meet the minimum emission requirement, including large and lightweight criteria. However, studies that have attempted to investigate the structural behaviour and design formulas for curved plates and stiffened panels are relatively limited (Park et al., 2009, 2011, 2018; Tran et al., 2012, 2014; Martins et al., 2013, 2014; Seo et al., 2016; Cho et al., 2018, 2019; Li and Kim, 2022; Li et al., 2022) comparing with the flat-plate and stiffened panel (Ueda et al., 1975, 1992; Tanaka and Endo, 1988; Fujikubo et al., 1997; Paik and Thayamballi, 1997; Fujikubo and Kaeding, 2002; Chen, 2003; Paik et al., 2004; Paik, 2007; Zhang and Khan, 2009; Khedmati et al., 2010; Kim et al., 2017, 2018b, 2019, 2020b; Xu et al., 2018).

Recently, studies related to the Ultimate Limit State (ULS) for flat-plate and stiffened panels have been continuously conducted by

several researchers. (Anyfantis, 2020; Li et al., 2021; Liu et al., 2021; Kim et al., 2022a, 2022b, 2023; Xu et al., 2022). Many more research outcomes exist if we consider the effective width or breadth concepts of the flat plate or flat stiffened panel. Hence, further investigations on the structural behaviour of unstiffened curved plates need to be carried out.

Paik (2018a, 2020) stresses that the failure to predict the structural behaviour, such as collapse strength or limit state of structural components, could lead to significant issues related to Health, Safety and Environment (HSE). Moreover, despite the continued effects, numerous incidents are still being reported. Therefore, the safety of structural components under various loading conditions shall be secured (Paik et al., 2012b; Kim et al., 2013b, 2020a; Youssef et al., 2016).

Many researchers have conducted several studies on the structural behaviour of the curved plate. In particular, the curved plate under compression topic was covered by several articles in terms of elastic and critical buckling stresses (Domb and Leigh, 2001; Martins et al., 2013; DNVGL, 2015; Martins et al., 2016) and ultimate strength performance (Tran et al., 2012, 2014; Seo et al., 2016; Park et al., 2018; Martins et al., 2014). Martins et al. (2018) recently provided a wide range of historical and technical reviews on the behaviour of curved plates under in-plane stresses.

The behaviour of the ultimate strength of plates or stiffened panels is influenced by various factors such as geometric properties, material properties, initial imperfection, boundary condition, and finite element (FE) modelling techniques, including mesh size, model size, and many others (ISSC, 2012; Paik et al., 2012a; Kim et al., 2018a). Curved plates with curvature or flank angle show more complex structural behaviours than flat plates due to the complex geometry effect when they progressively collapse.

Several existing design formulas and guidelines are used to evaluate the curved plate's elastic buckling and ultimate strength. However, it may be further improved and refined by considering detailed geometric characteristics such as flank angle (or the curvature effect), plate aspect ratio, and plate slenderness ratio, and these are considered the main objectives of the present study.

Therefore, the objective of the present study can be summarised as follows.

- To propose and validate an empirical formula to predict the ultimate strength of unstiffened curved plates.
- To investigate the effect of parameters consisting of cylindrically curved plates on the Ultimate Limit State (ULS) behaviour.

The scope of this study is limited to the following constraints.

- Loading condition is limited only to longitudinal compression load
- Limited to average severity of initial imperfection. The effect of welding residual stress is neglected.
- Analysis of ultimate strength behaviour is limited to steel curved plates (MS24 and AH32).
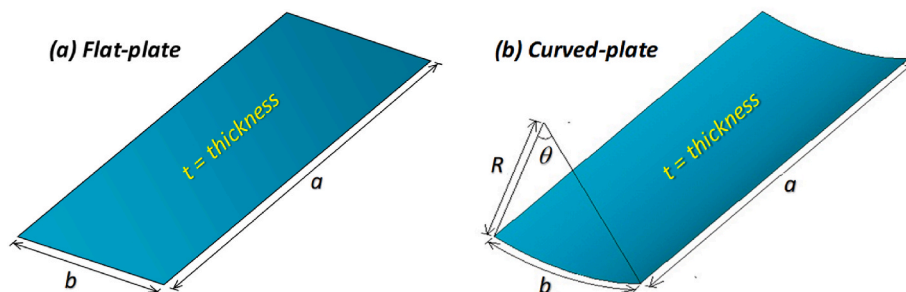
- The proposed empirical formula for the curved plate is limited to a specific range of flank angle (θ), plate aspect ratio (a/b) and slenderness ratio (β) defined in this study.

2. Technical reviews of previous studies and design formulas

There are a number of empirical formulas for predicting the ultimate strength of flat-plate subjected to longitudinal compression. Most of the formulas are derived as a function of the plate slenderness ratio ($\beta = (b/t)\sqrt{\sigma_Y/E}$), including the effect of geometric and material properties shown in Fig. 1(a). Furthermore, initial imperfections (i.e., initial deflection, welding-induced residual stress, and others), accidently damaged (i.e., grounding, collision, dropped objects, fire, explosion, etc.), artificially produced (i.e., hole, cutout, etc.) and many other conditions can also consider by supplementing additional coefficients.

In the case of the curved plate in Fig. 1(b)(b), existing formulas are relatively limited compared to the flat-plate. Some formulas are developed by modifying the flat-plate formula, as shown in Eq. (1). In addition, the empirical formula adopts the basic parameters as shown in Eq. (2).

Frankland (1940) proposed a formula for predicting the ultimate strength of the clamped plate, as illustrated in Eq. (1).

$$\frac{\sigma_{xu}}{\sigma_Y} = \begin{cases} 1.0 \ for \ \beta < 1.25 \\ \dfrac{2.5}{\beta} - \dfrac{1.5625}{\beta^2} \ for \ \beta \geq 1.25 \end{cases} \tag{Eq. 1}$$

An empirical formula by Maeno et al. (2004).

$$\frac{\sigma_{xu}}{\sigma_Y} = a\left(\frac{R}{t} - 40\right)^2 + 0.983 \tag{Eq. 2}$$

where, $a = -0.6\left(\frac{\sigma_Y}{E}\right)^2 + 0.0046\left(\frac{\sigma_Y}{E}\right) - 0.24(10^{-6})$.

Maeno et al. (2004) proposed an empirical formula to estimate the ultimate strength in terms of the radius/thickness ratio and the yield stress. The radius/thickness ratio and the yield stress of the material will influence the ultimate strength of the bilge circle.

Modified Faulkner's formula by Park et al. (2009, 2018).

$$\frac{\sigma_{xu}}{\sigma_Y} = \begin{cases} 1.0 \ for \ \beta < 1.0 \\ \dfrac{2}{(\beta')} - \dfrac{1}{(\beta')^2} \ for \ \beta \geq 1.0 \end{cases} \tag{Eq. 3}$$

where, $\beta' = \beta \times \sqrt{\frac{\sigma_{cr}^{Flat}}{\sigma_{cr}^{Curve}}} = \beta \times \sqrt{\frac{\sigma_u^{Flat}}{\sigma_u^{Curve}}}$.

Based on the general shape of the formula in Eq. (1), Faulkner (1975) and Guedes Soares (1988) proposed similar empirical formulas. Furthermore, Faulkner's formula is also utilised by Park et al. (2009, 2018), as shown in Eq. (3). Park et al. (2009, 2018) introduced a new definition of slenderness parameter (β') by considering the ratio of the elastic-plastic buckling and ultimate strength of flat plate to those of curved plate. β' is substituted into Faulkner's formula of ultimate strength for a flat plate. The modified Faulkner's formula can estimate a

Fig. 1. Schematic view of the flat- and curved plates (Note: a = plate length, b = plate breadth, t = plate thickness, R = radius, and θ = flank angle).

curved plate's ultimate strength with a relatively small flank angle under longitudinal compression.

Recently, Kim et al. (2014) proposed the empirical formula in Eq. (4) by adding a sub-coefficient (C_F) to consider the effect of curvature. The C_F can be calculated by following Eqs. (4a) to (4c).

$$\frac{\sigma_{xu}}{\sigma_Y} = C_F \times \left(\frac{2.25}{\beta} - \frac{1.25}{\beta^2}\right) \tag{Eq. 4}$$

where, $C_F = \frac{C_a}{\beta^2} + \frac{C_b}{\beta} + C_c$;

$$C_a = 3.434\left(\frac{b}{R}\right)^2 - 1.989\left(\frac{b}{R}\right) + 0.646 \tag{Eq. 4a}$$

$$C_b = -4.138\left(\frac{b}{R}\right)^2 + 1.934\left(\frac{b}{R}\right) - 1.023 \tag{Eq. 4b}$$

$$C_c = 1.001\left(\frac{b}{R}\right)^2 - 0.181\left(\frac{b}{R}\right) + 1.382 \tag{Eq. 4c}$$

In Kim et al. (2014)'s original paper, they express the sub-equations in Eqs. (4a) to (4c) as a function of R/t. However, we assume that it is a typo and b/R might be the correct expression rather than R/t. Kim et al. (2014) did not provide the applicable range of the β, but the ULS value should be fixed to 1.0 when β is less than 1.25, as illustrated in Eq. (3).

The comparison section will discuss the difference between each empirical formula based on statistical analysis. Recently, Kim et al. (2021) conducted experimental studies on cylindrically curved plates. This study will also compare the testing results with the developed empirical formula in the validation section.

Many other studies have also been conducted to investigate the structural behaviour of thin-walled curved plates, and a detailed review may be referred to Martins et al. (2018). Also, most of the studies adopted the curvature parameter or developed a formula based on the plate's critical buckling strength shown in Eq. (5). However, we attempt to expand the plate slenderness ratio to express the curved plate's ultimate strength performance by adding the flank angle variable in this study.

$$\sigma_{cr} = f \cdot \sigma_E \tag{Eq. 5}$$

where, σ_{cr} = critical buckling strength of the plate, σ_E = elastic buckling strength of the plate, f = correction factor to consider the curvature effect and boundary condition. Details can refer to Martins et al. (2018).

3. Methodology

The objective of the study is the formulation of the ultimate strength of an unstiffened curved plate. The ANSYS NLFEM, one of the famous numerical codes, is applied to assess the ultimate strength of an unstiffened curved plate under longitudinal compression. Currently, NLFEM is considered the most efficient and cost-effective method for providing precise solutions. The refined formula can be developed using the ultimate strength of the unstiffened curved plate from ANSYS NLFEM through the regression method to predict the unstiffened curved plate's ultimate strength. Therefore, it is essential to assess the unstiffened curved plate using ANSYS NLFEM to be precise in developing an advanced formula.

It is necessary to foresee possible uncertainty factors in modelling an unstiffened curved plate that might affect the FE analysis to represent the actual structural behaviour. The applied NLFEM modelling technique should be able to represent the actual structural behaviour corresponding to geometric and material nonlinearity, boundary and loading conditions, type and magnitude of initial imperfections, mesh size and others. The flowchart in Fig. 2 presents the overall procedure of the present study and can be divided into three main parts: the modelling details, structural assessment and formulation, including validation.

The proposed methodology summarised in Fig. 2 can also be applicable for developing the empirical formula for predicting the ultimate limit state of the unstiffened (i.e., curved or flat plate) and stiffened panels. In brief, the overall procedure is similar to the general finite element analysis (FEA), including the (a) pre-processing (data collection and characterisation: material and geometric, definition of the applied loads, selection of the reliable scenarios), (b) analysis (numerical simulation by NLFEM but this may be replaced by experimental
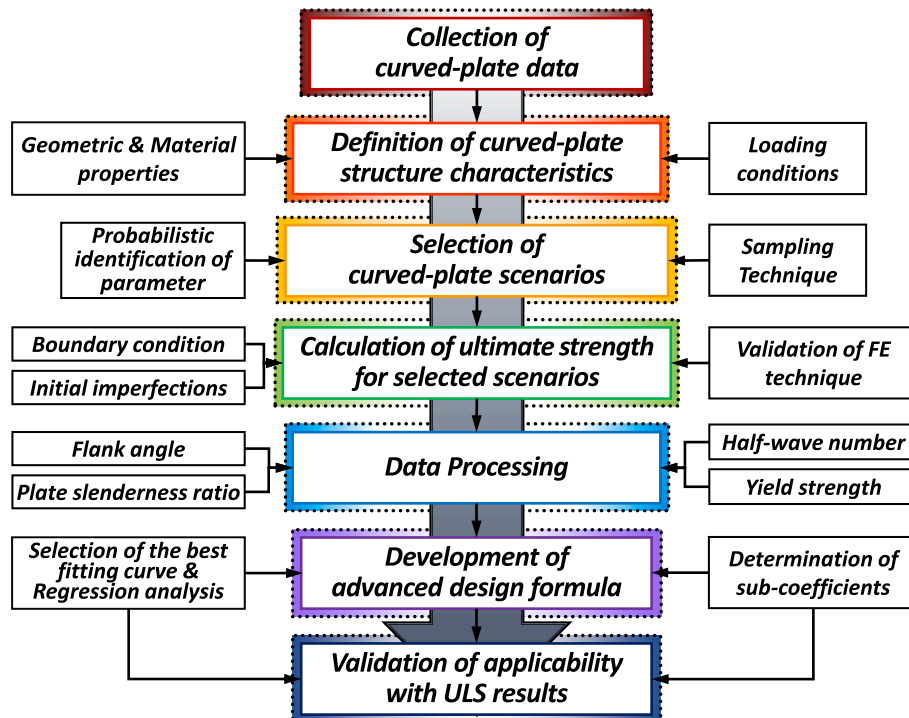

Fig. 2. Flowchart for the development of a practical and simplified formula of the curved plate.

investigation), and (c) post-processing (development of the formula and verification).

The generated data by ANSYS, a well-known commercial numerical simulation code, can quantify the ultimate structural strength capacity of an unstiffened curved plate and investigate the effects of the essential parameters in the design of the unstiffened curved plate. The applicability of the obtained formula is verified by statistical analysis with NLFEM results.

3.1. Collection of the curved plate data and definition of the structural characteristic

Several studies have been conducted previously to determine the reliable range of plate modelling by FEM. In the present study, a one-bay and one-span plate model is adopted for FE simulation. A cylindrically curved plate can be defined by geometric and material properties. It has dimensions of length (a), breadth (b), plate thickness (t), flank angle (θ), as shown in Fig. 1(b). The radius (R) can be calculated when the breadth and flank angle information is given, i.e., $b = R\theta$. Either flank angle or radius parameter is generally used in developing an empirical formula. In this study, we adopted the flank angle as a key parameter. The material yield strength (σ_Y) and Elastic modulus (E) should be needed for the FE analysis.

3.2. Selection of curved plate scenarios

There is limited information on the curved plate geometry and material properties. Therefore, we referred to flat-plate data from Kim et al. (2018b) and considered flank angle data for research purposes. A 3D shape surface curve can express the expected outcome of this study as follows.

- x-axis: plate slenderness ratio (β), which is a function of material and geometric properties
- y-axis: flank angle (θ)
- z-axis: normalised ultimate strength capacity of the curved plates in longitudinal compression (σ_{xu}/σ_Y)

The details, including selected scenarios, will be shown in section 4.

3.3. Calculation of ultimate strength for selected scenarios

Enormous demands develop several commercialised numerical simulation codes available nowadays, such as ANSYS, Abaqus, LS-Dyna, and many others. They are considered full NLFEM, and individuals also develop simplified software to get user-friendly solutions from classification societies, shipyards, and others.

The present study uses the ANSYS nonlinear finite element method (NLFEM). A detailed procedure to calculate the ultimate limit state of the selected curved plate scenarios is summarised in this section.

3.3.1. ANSYS nonlinear FE simulation code and input data

Although all shell elements in the ANSYS element library generally can be used to model unstiffened curved plate structural behaviour, the SHELL181 element was selected to model the plates as it is considered the most preferred for the proposed FE analysis for thin-walled structures. It has four nodes with six degrees of freedom per node; translation in the x, y, and z directions and rotation about x, y, and z-axes (ANSYS, 2014). The selected element shall be able to model the structural behaviour in both the linear and nonlinear regions, including large displacement, elastic-plastic deformations and associated plasticity effects.

In most cases, the classical metal plasticity model in the ANSYS library is suitable for general collapse analysis. An appropriate material nonlinearity model should be selected as it is crucial to stimulate the yielding of plastic deformation. In the present study, the material model

for curved plates used nonlinear inelastic with isotropic hardening plasticity rule incorporating the von Mises yield surface model. Due to the possibility of large deformation and finite strains during the analysis, the elastic-perfectly plastic stress-strain relationship is defined by material properties: Elastic modulus of 205.8 GPa, Poisson ratio of 0.3, the yield stress of 235 MPa and 315 MPa. Zero tangent modulus was used for the pessimistic strength assessment result. In solution control, automatic large displacement control with the arc-length method is used.

3.3.2. Boundary condition and applied load

The NLFEM analysis is carried out using the one-bay model extent in this study. In general, the one-span model is adopted to investigate the structural behaviour under longitudinal compression. It is recognised that structural engineers should decide how to select the appropriate model extent and related boundary condition prior to conducting FE simulation. It is recognised that ½+½ model is also applicable as an effective way to investigate the ultimate strength and buckling behaviour of the continuous plate, including the effect of the transverse frame's torsional rigidity. In addition, two-bay models (½+1+½ or 1 + 1) or three-bay models (½+1 + 1+½ or 1 + 1+1) may also be recommended (ISSC, 2012; Paik et al., 2012a; Kim et al., 2013a). Two- or three-bay models may provide better accuracy by considering the rotational restraint from the modelled supporting members. However, the one-bay model is adopted to get a cost-effective solution by reducing the computation cost (Paik et al., 2012a; Park et al., 2018).

The simply-supported (SS) plate is considered the worst condition (or pessimistic design scenario), which allows maximum deflection, but it enables it to secure an additional structural safety margin (Paik, 2018a). It is known that SS gives more conservative results compared to other conditions, such as clamped (CL) boundary conditions. The ultimate strength of plates under the CL condition will be higher than that of plates under the SS condition. However, the boundary condition of the plate in the ship structure is neither SS nor clamped condition in an actual situation. It is between SS and CL conditions (Paik et al., 2012a). The applied load (= longitudinal compression), model extent (=one-bay and one-span model), and boundary condition (= simply supported) are presented in Fig. 3.

The edge condition of the plating in a continuous stiffened-plate structure, used in ships and offshore structures, is neither simply supported nor clamped, as mentioned in Paik et al. (2012b). Because the torsional rigidity of the support members at the plate edges is neither zero nor infinite. In a robust ship and offshore structural design, it is necessary to accurately take into account the effect of the edge condition in analyses of plate behaviour in terms of buckling and post-buckling behaviour.

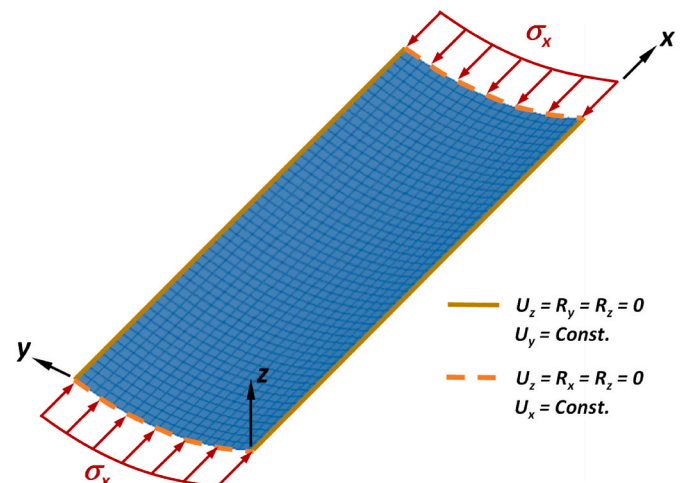The simply support boundary condition may allow the confirmation

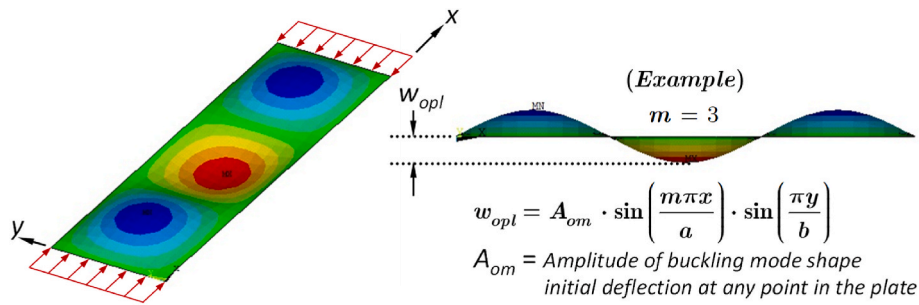**Fig. 3.** Simply supported boundary condition.

Fig. 4. Visualised initially deflected plate based on buckling mode presented in Ep. 6a.

of the worst or pessimistic ULS (ultimate limit state) values, which can also support securing the additional safety margin. The adopted boundary condition (Uz = Ry = Rz = 0 in the global Cartesian coordinate system) for curved plate is not a perfectly simply supported condition (The vertical support condition, e.g., Uz should always be perpendicular to the face or supported line). However, it may be closed to the SS condition rather than clamped.

3.3.3. Initial imperfections

Initial imperfection is known to be the source of imperfect correlation between theoretical and actual results. Several studies have been conducted to consider the actual condition; however, it still needs to be investigated further to minimise the uncertainties caused by the fabrication process. Therefore, initial imperfection needs to be included in the FE analysis to replicate the actual condition and collapse behaviour of the structure. Residual stress and initial deflection, generally considered a major initial imperfection, exist during the fabrication and manufacturing processes. Generally, five different initial deflection shapes are adopted, which are 1) Hungry horse mode, 2) Mountain mode, 3) Spoon mode, 4) Sinusoidal mode, and 5) Buckling mode (Paik, 2018b). The presence of initial imperfection generally decreases the ultimate strength capacity of the structures.

Martins et al. (2015) presented a study on the sensitivity of initial imperfections of cylindrically curved plates. They concluded that imperfections in cylindrically curved plates are not covered accurately enough in the current standards and proven that cylindrically curved plates are highly sensitive to initial imperfections. Additionally, the ultimate strength performance becomes more sensitive to initial imperfection amplitude as the curvature parameter increases.

For flat plate, the implication of initial imperfection is being done by reassigning the nodal points coordinate through programming code. The imperfection coordinate of nodal points can be produced by the buckling mode initial deflection equation shown in Eq. (6a) and Fig. 4. The reassignment of nodal point coordinates to consider initial deflection should be applied, and it is called geometry update, in general. Eigenvalue analysis is also an available option to provide the same results for the geometry update. In the present study, welding-induced residual stress is not considered, and only the effect of average severity of initial deflection for plate is considered. The plate initial deflection is represented as follows:

$$w_{opl} = A_{om} \cdot \sin\left(\frac{m\pi x}{a}\right) \cdot \sin\left(\frac{\pi y}{b}\right) \tag{Eq. 6a}$$

where A_{om} = amplitude of the buckling mode shape initial deflection under longitudinal compression, m = buckling mode half-wave number of the plate in the longitudinal direction (x) defining as a minimum integer which satisfies $a/b = \sqrt{m(m+1)}$, a = length of the plate, b = breadth of the plate (=θ × R), x, y = longitudinal and transverse axis, respectively. An example may be referred to as Fig. 4(b) = θ × R.

For the buckling mode initial deflection of plate (=w_{opl}), it can be mathematically expressed by Eq. (6a). The A_{om} presents the amplitude of the equation in Eq. (6b) so that maximum amplitude should be

considered as the buckling mode initial deflection.

Smith et al. (1988) suggested three (3) levels of initial deflection, such as slight, average, and several, by adopting a hungry horse mode shape, as shown in Eq. (6c). The suggested values may be applicable for many types of initial deflection shapes for practical purpose with the benefit of mathematical simplicity.

$$A_{om} = C_{ID} \cdot \beta^2 \cdot t \tag{Eq. 6b}$$

where, C_{ID} = initial deflection coefficient as shown in Eq. (6c).

$$C_{ID} = \begin{cases} 0.025 \text{ for slight level} \\ 0.10 \text{ for average level} \\ 0.30 \text{ for severe level} \end{cases} \tag{Eq. 6c}$$

For the flat- and curved plate, eigenvalue buckling analysis is performed to imply initial deflection on the plate. Fig. 5 shows the initial deflection shape selected by the lowest eigenvalue through an elastic buckling analysis under longitudinal compression. The unit compressive load applies to the short edges of the plate. The magnitude of initial imperfection is multiplied by the average level of initial deflection ($w_{opl} = 0.1\beta^2 t$). The elastic buckling mode shape differs according to the flank angle of the plate, as shown in Fig. 5(b), (c), and (d).

3.3.4. Validation of the FE modelling technique

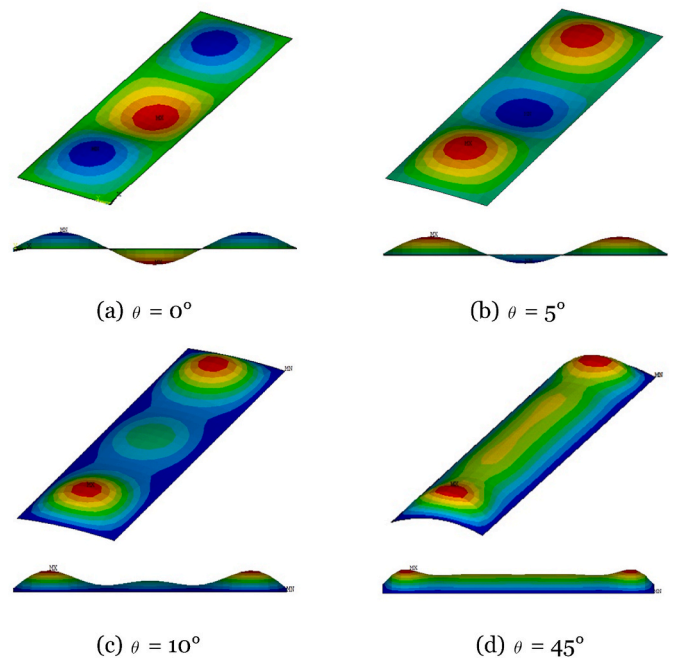Fig. 6 shows an example of ULS analysis and von-Mises stress

(a) θ = 0°   (b) θ = 5°

(c) θ = 10°   (d) θ = 45°

Fig. 5. Typical examples of the initially deflected plates in longitudinal compression: (a) flat-plate, (b) to (d) curved plates.
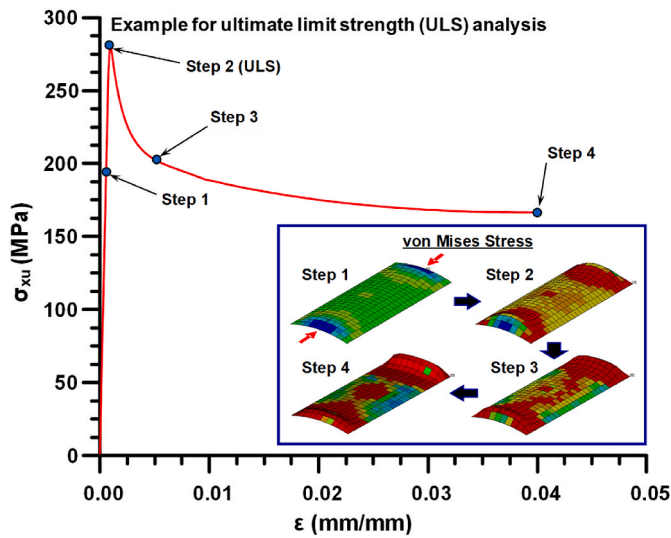
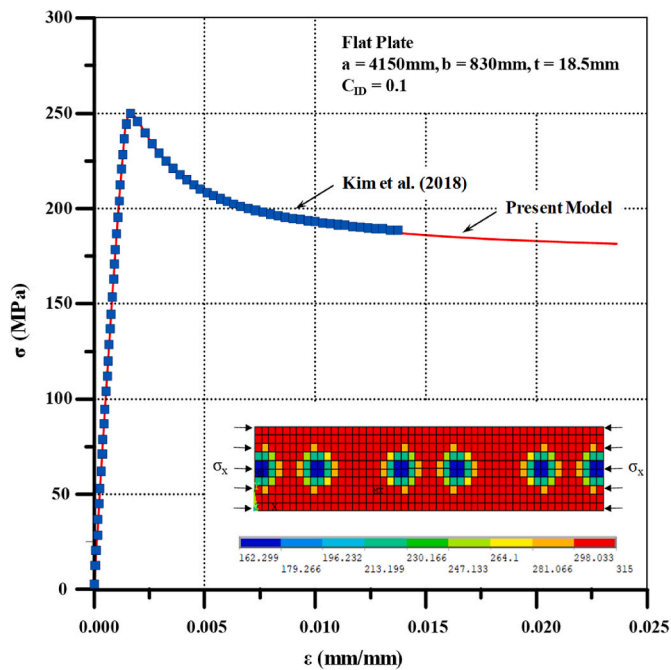**Fig. 6.** A typical example of ULS analysis for the curved plate.

Fig. 7. Validation of the FE modelling technique applied to flat-plate.

Fig. 8. Validation of the FE modelling technique applied to curved plate.

extracted from different incremental step of the FE analysis. The load shortening curve, which combines von-Mises stress and strain, enables determining whether the plate reaches the elastic proportional limit, ultimate limit, fracture, etc. The deformation of the plate can also be monitored through the steps in Fig. 6. Step 1 shows the pre-buckling state; Step 2 shows the ULS state; Step 3 and 4 shows the post-buckling state. In FEM, the highlighted red colour is where the plate experiences close to yield stress and where most failure may occur.

3.3.4.1. For flat-plate. The modelling technique must be validated to provide a reliable and accurate result. For the flat-plate, the load-shortening curves are compared through benchmarking with Kim et al. (2018b), shown in Fig. 7. Both models used the same geometric and material properties. The present model has an ultimate strength of 249.82 MPa, while Kim et al. (2018b)'s model has 249.80 MPa. The difference is close to zero, which indicates that the NLFEM technique
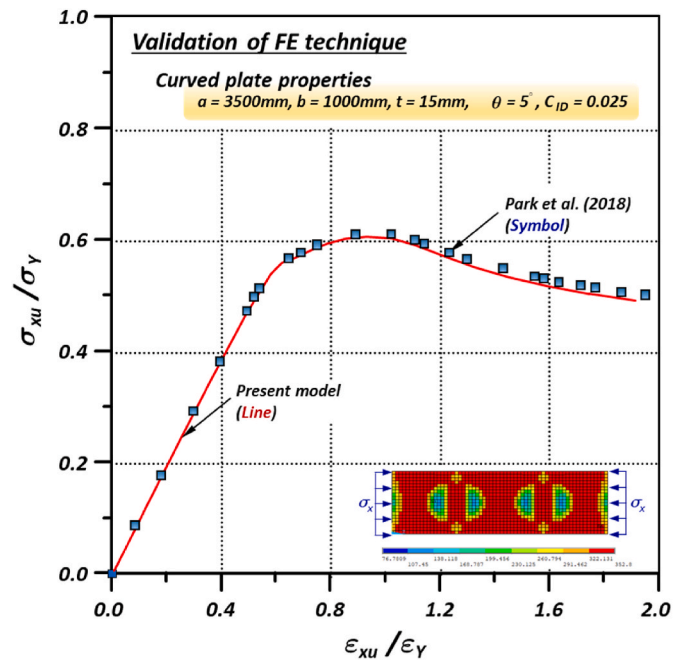
used in this study is acceptable. Since the modelling technique is validated now, the parametric study can be conducted by considering reliable scenarios of the flat-plate.

3.3.4.2. For curved plate. For the curved plate, the model is validated with the typical result by Park et al. (2018) presented in Fig. 8, which shows the normalised stress versus average strain curve. The present model includes initial imperfection and uses the same material model. The normalised ultimate limit states by yield strength (=σ_{xu}/σ_Y) were 0.601 and 0.602 by the present model and Park et al. (2018), respectively. The difference is approximately 0.06%, which indicates that the present FE technique is applicable. Since the modelling technique was developed and validated, the ultimate strength of the curved plate can be determined using the same modelling technique with different material and geometric properties.

3.4. Data processing

Prior to developing the empirical formula for predicting the ultimate strength of the flat- and curved plate, the entire input data should be processed to get the optimised outcome. In this study, regression analysis should be conducted based on the suggested parameters, which can express the flat- and curved plate, described in section 3.2. Therefore, the expected outcome (or normalised ULS = σ_{xu}/σ_Y) is going to be a function of plate slenderness ratio (β) and flank angle (θ) by regression analysis, as shown in Eq. (7).

$$\sigma_{xu} / \sigma_Y = f(\beta, \theta) \qquad \text{(Eq. 7)}$$

The good thing is that the plate slenderness ratio ($\beta = b/t \cdot \sqrt{\sigma_Y/E}$) includes the effect of material and geometric properties, so multivariable nonlinear regression is not required. Based on the data processing results, the best-fitting curve can be selected as the proposed empirical formula.

3.5. Development of empirical formula

There might be limitations to expressing the actual ULS behaviour by developed empirical formulas mentioned in the introduction section. For example, Eq. (1) by Maeno et al. (2004), which is a form of the
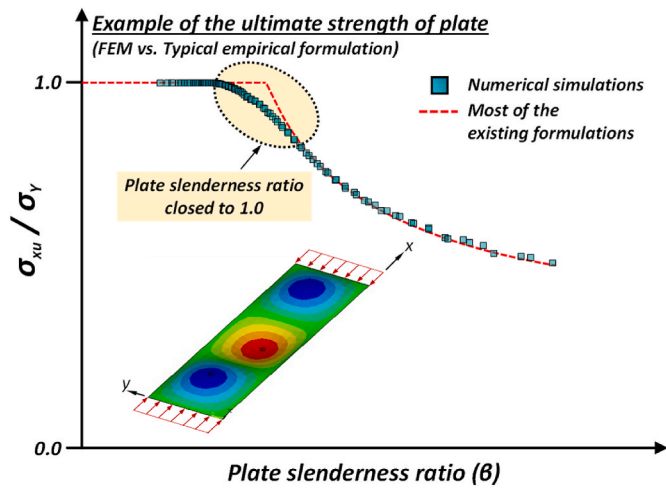
Fig. 9. Limitation of the existing design formulas.

quadratic function, limits the ULS value at the starting point that does not satisfy 1.0. Furthermore, Eqs. (2) and (3) are being expressed by two regions based on β highlighted in Fig. 9. Other empirical formulas (Park et al., 2018; Kim et al., 2014) can be considered similar above.

Recently, Kim et al. (2018b) proposed an advanced empirical formula shown in Eq. (8) to predict the ultimate strength of the initially deflected flat-plate by buckling mode shape subjected to longitudinal compression. They adopted the initial deflection index concept (IDI), a function of plate slenderness ratio, including sub-coefficients (c_1 to c_4).

Equation (8) could express the ultimate limit state (ULS) smoothly near the boundary region where the plate slenderness ratio (β) is closed to 1.0 in Fig. 9. They confirmed that the proposed empirical formula is applicable in predicting the ultimate strength behaviour, including the effect of buckling mode shape initial deflection and its amount.

Nevertheless, the obtained outcome only applied to the flat-plate, and the curved plate is further investigated in this study. The present study aims to propose an advanced empirical formulation to predict the curved plate's ultimate strength under longitudinal compression by considering the flank angle (θ) effect. Besides, the effect of the plate's aspect ratio on the ULS is further analysed.

$$\frac{\sigma_{xu}}{\sigma_Y} = 1 - e^{IDI} \qquad \text{(Eq. 8)}$$

where, $IDI = initial\ deflection\ index\left(= \frac{c_1}{\beta} + \frac{c_2}{\beta^2} + \frac{c_3}{\beta^3} + c_4 \right)$;

$\beta = plate\ slenderness\ ratio\left(= \frac{b}{t}\sqrt{\frac{\sigma_Y}{E}} \right)$; $c_1\ to\ c_4 = sub-coefficients$ which are closely related to the buckling mode initial deflection.

In most cases, design curves are shaped like a 2D diagram of horizontal and vertical axes. The expected outcome is presented on the vertical axis, while the summarised design inputs are shown on the horizontal axis. Therefore, a design variable considering the target structure's material and geometric properties should be clearly defined. In this regard, we recognised that plate slenderness ratio (β) and column slenderness ratio (λ) are adopted to predict the ultimate strength of the unstiffened plate and stiffened panel, respectively.

Various studies (Lin, 1985; Paik and Thayamballi, 1997; Zhang and Khan, 2009; Kim et al., 2017) proposed an empirical formulation to estimate the ULS of the stiffened panel by combining β and λ. Furthermore, Kim et al. (2019; 2020b) developed advanced empirical formulations by multivariable regression analysis and found that additional variables (h_w/t_w and I_{pz}/I_{sz}) may enable the prediction of the ULS of the stiffened panel accurately. The present study only works out for the unstiffened panel (=plate) matter, so the stiffened panel will not be discussed further here.

As shown in Eq. (8), the plate slenderness ratio is a function of material properties (b and t) and geometric properties (σ_Y and E). In addition, the buckling shape initial deflection of the plate could be considered by the four sub-coefficients (c_1 to c_4). In the case of a curved plate, the effect of the flank angle (θ) can be presented by sub-coefficients (f_1 to f_4), which are expressed differently to avoid confusion from the previous study outcome. Therefore, the expected shape of this study's empirical formulation is shown as given by Eq. (9).

$$\frac{\sigma_{xu}}{\sigma_Y} = 1 - \exp\left(\frac{f_1}{\beta} + \frac{f_2}{\beta^2} + \frac{f_3}{\beta^3} + f_4\right) \qquad \text{(Eq. 9)}$$

where, $f_1\ to\ f_4$ = sub-coefficients which are the function of flank angle.

3.6. Statistical analysis for the validation of the applicability of the developed formulation

The accuracy of the developed empirical formulation should be validated by statistical analysis. In general, the coefficient of determination (R^2), mean (M), and coefficient of variation (COV) are widely used to confirm its applicability. In section 4, this will be conducted and validated.

4. Development of empirical formulation based on the parametric study

4.1. Selection of plate scenarios

As mentioned above, the flank angle (θ), plate aspect ratio (α) and slenderness ratio (β) are set as the basic parameters to investigate the ultimate strength performance of the flat- and curved plate and the obtained outcomes are used to develop the empirical formulation in this study. To reduce the complexity, the fixed mean values of plate breath (=830 mm) and material elastic modulus (=205800 MPa) are adopted as suggested by Kim et al. (2018b), while the other parameters (a, t, σ_Y) are changed so that effectively distributed β can be obtained, as shown in Table 1.

The plate aspect ratio (α) is selected as 2.0 and 5.0 by considering the mid-ship section's bilge part, while the flank angle (θ) ranges from 0° to 45°. In the case of yield strength (σ_Y), two representative values used in shipbuilding, such as 235 MPa (Mild steel, MS24) and 315 MPa (High tensile steel, HT32), are selected. The selected plate scenarios are summarised in Table 1. A total of four hundred (400) plate scenarios were chosen.

Table 1
Selected scenarios for the numerical simulation by NLFEM.

a (mm)	b (mm)	t (mm)	θ (deg.)	σ_Y (MPa)	E (GPa)	β
1660 &4150	830	44.5	0	315	205.8	0.73
		38.5	5			0.84
		34.0	10			0.96
		30.0	15			1.08
		26.0	20			1.25
		22.0	25			1.48
		18.5	30			1.76
		15.5	35			2.09
		12.0	40			2.71
		8.5	45			3.82
		42.0		235		0.67
		36.5				0.77
		32.0				0.88
		28.5				0.98
		24.0				1.17
		20.0				1.40
		16.5				1.70
		13.5				2.08
		10.0				2.80
		7.0				4.01

Total number of scenarios

$\underset{a}{2} \times \underset{b}{1} \times \underset{t}{10} \times \underset{\theta}{10} \times \underset{\sigma_Y}{2} \times \underset{E}{1} = 400\ scenarios$

4.2. Analysis of the individual parameters and their effects on the ULS

Prior to developing the empirical formulation, it is necessary to analyse the effect of each variable, i.e., plate aspect ratio, material yield strength, and flank angle, on the ultimate limit state of the plate. Analysed information may be applied to determine the coefficient of sub-coefficients, as presented in Eq. (9).

4.2.1. Effect of plate aspect ratio and material yield strength

Once numerical simulations are completed by the ANSYS NLFEM for the selected 400 plate scenarios, the ULS behaviours can be plotted in the 2D diagram as the plate slenderness ratio increases. In advance, we investigate the effect of plate aspect ratio and material yield strength by plotting the detailed 2D diagrams, as shown in Figs. 10 and 11. We split diagrams based on the flank angle to manage a wide range of information for data processing.
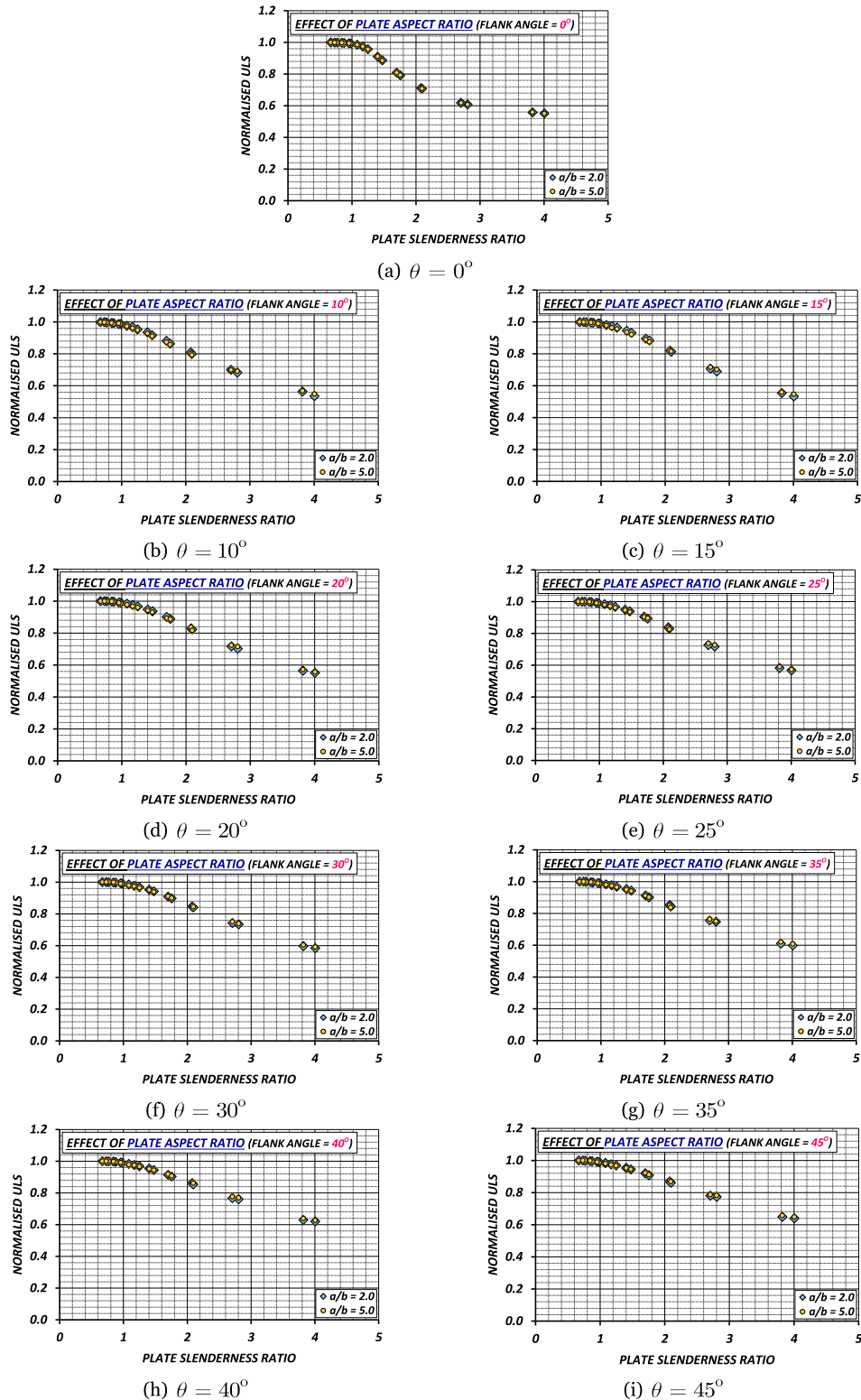

(a) $\theta = 0^{\circ}$

(b) $\theta = 10^{\circ}$

(c) $\theta = 15^{\circ}$

(d) $\theta = 20^{\circ}$

(e) $\theta = 25^{\circ}$

(f) $\theta = 30^{\circ}$

(g) $\theta = 35^{\circ}$

(h) $\theta = 40^{\circ}$

(i) $\theta = 45^{\circ}$

Fig. 10. Effect of plate aspect ratio on the ultimate strength performance.

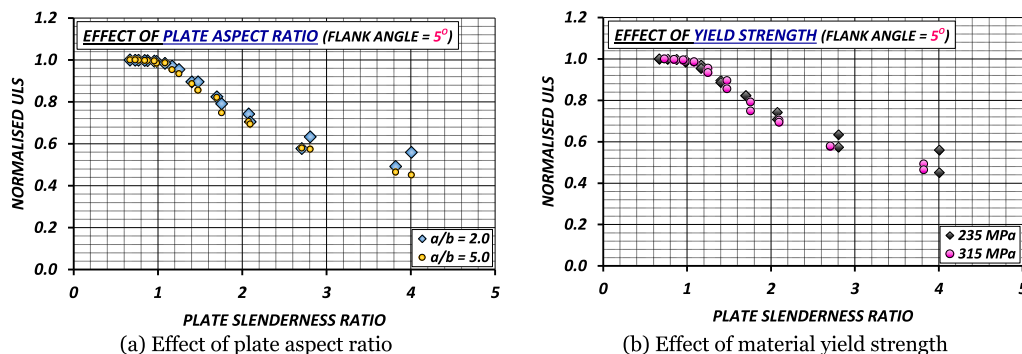(a) Effect of plate aspect ratio   (b) Effect of material yield strength

Fig. 11. Comparison of the ULS values at 5° of flank angle.

In Fig. 10, we plotted FE results based on the plate aspect ratio (a/b) in the 2D diagram. Again, we selected 2.0 and 5.0 of a/b presented in Table 1. In most cases in Fig. 10, the obtained FE results (= ULS in here) plotted closely with each other except for the case of five degrees (5°) of the flank angle, as shown in Fig. 11(a). As Park et al. (2018) stated, this might be caused by the deflection shape changes at the small flank angle as the compressive load increases. On the other hand, the ULS has a sensitive response in the small flank angle range.

Fig. 11(a) clearly detects the fluctuation behaviour of the ULS, which reminds us that there is uncertainty in investigating the actual ULS behaviour in the small flank angle. The obtained outcome in Fig. 11(a) shows a relatively good agreement when the plate is thick ($\beta < 1.8$), while the difference between a/b = 2.0 and 5.0 increases as the plate is thinner ($\beta \geq 1.8$). This should be further investigated in the future by selecting the precise range of the small flank angle (0° to 10°).

In the case of plate aspect ratio results in Figs. 10 and 11(a), the same values applied in the horizontal axis (= plate slenderness ratio) for both $a/b = 2.0$ and 5.0. Therefore, the similarity was able to be compared directly. We continue to analyse the effects of material yield strength on the ULS in Figs. 11(b) and Fig. 12 by comparing the 2D diagrams, which are the relationship between the plate slenderness ratio and the ULS, as the flank angle increased. However, the selected scenarios in Table 1 do not have the same value on the horizontal axis (= plate slenderness ratio). This is because the plate slenderness ratio ($\beta = b/t \cdot (\sigma_Y/E)$) is affected by geometric and material properties. In particular, we fixed plate breadth (b) and the Elastic modulus (E) while the plate thickness (t) varies. In addition, the plate length is not taken into account for the calculation of β. Therefore, the direct comparison of the ULS values between 235 MPa and 315 MPa is not available, as shown in Figs. 11(b) and 12.

Nevertheless, we recognised the smoothly decreasing trend of ULS as β increased from the previous studies and numerical simulation results in Fig. 10. It seems that the ULS values shown in Fig. 12(a)-(i) combined by 235 and 315 MPa could generate smooth fitting curves except for the case of $\theta = 5°$.

An interesting investigation may be available by comparing the cases of $\theta = 5°$, as illustrated in Fig. 11(a) and (b), even if we do not conduct various FE simulations to consider the wide range of scenarios. First of all, there might be a possibility to consider the effect of plate aspect ratio and material yield strength in the lower range of flank angle. Lower plate aspect ratio and yield strength tend to be more sensitive as the plate gets thick, as shown in Fig. 11(a) and (b). A detailed investigation may be further required in the future by selecting additional scenarios.

4.2.2. Effect of flank angle

The effects of plate aspect ratio and material yield strength were insignificant. It means that combined data can be utilised to develop empirical formulation. The effect of the flank angle is investigated in a similar context, as shown in Fig. 13. First of all, the ULS behaves differently between flat-plate ($\theta = 0$) and curved plate ($\theta > 0$).

In general, the trend line of the curved plates, representing the ultimate strength performance as plate slenderness ratio increased, tend to increase in the range of $10° < \theta \leq 45°$ at a similar late. In addition, the ULS of the curved plates tends to drop smoothly once β exceeds 1.0. This behaviour is generally observed for most curved plates except for small flank angle cases ($0° < \theta \leq 10°$). While the ULS of flat-plate tends to drop rapidly when β exceeds 1.0, which is earlier than curved plate. In contrast, the ULS reduction rate in flat-plate is mitigated as β closes to 3.0, while the decreasing trend in curved plate is constantly observed even β exceeds 3.0 or closed to 4.0.

The interesting behaviour is found when the flank angle (θ) is 5°, representing the small flank angle case in this study, as presented in the lowest trend line in Fig. 13. First of all, the ULS trend line for 5° curved plate placed lower region than the flat plate ($\theta = 0°$). However, the general trend is similar to the other curved plate cases except for the rapid dropping phenomenon. The detailed investigation results w.r.t. flank angle of 5° may referred to Kim et al. (2023) on page 414. In brief, the primary reason is that "A significant change is captured when it follows the secondary buckling path by changing deflection shape" (Kim et al., 2023).

When the flank angle increased to 10°, the trendline is near the other curved plate results ($15° \leq \theta \leq 45°$), but it still shows intermediate behaviour regarding the reduction rate mitigation when β closed to 4.0. Again, the detailed structural behaviour in the small flank angle should be further investigated in future studies.

4.3. Development of the empirical formulation based on processed data

From the previous section, the obtained outcome to developing the empirical formulation can be summarised as follows.

- The flank angle should be considered as an essential parameter.
- The effect of plate aspect ratio and material yield strength may be neglected (Note: This is assumed for selected scenarios only).
- The ULS behaviours at the small flank angle need to be further investigated by adopting detailed scenarios.

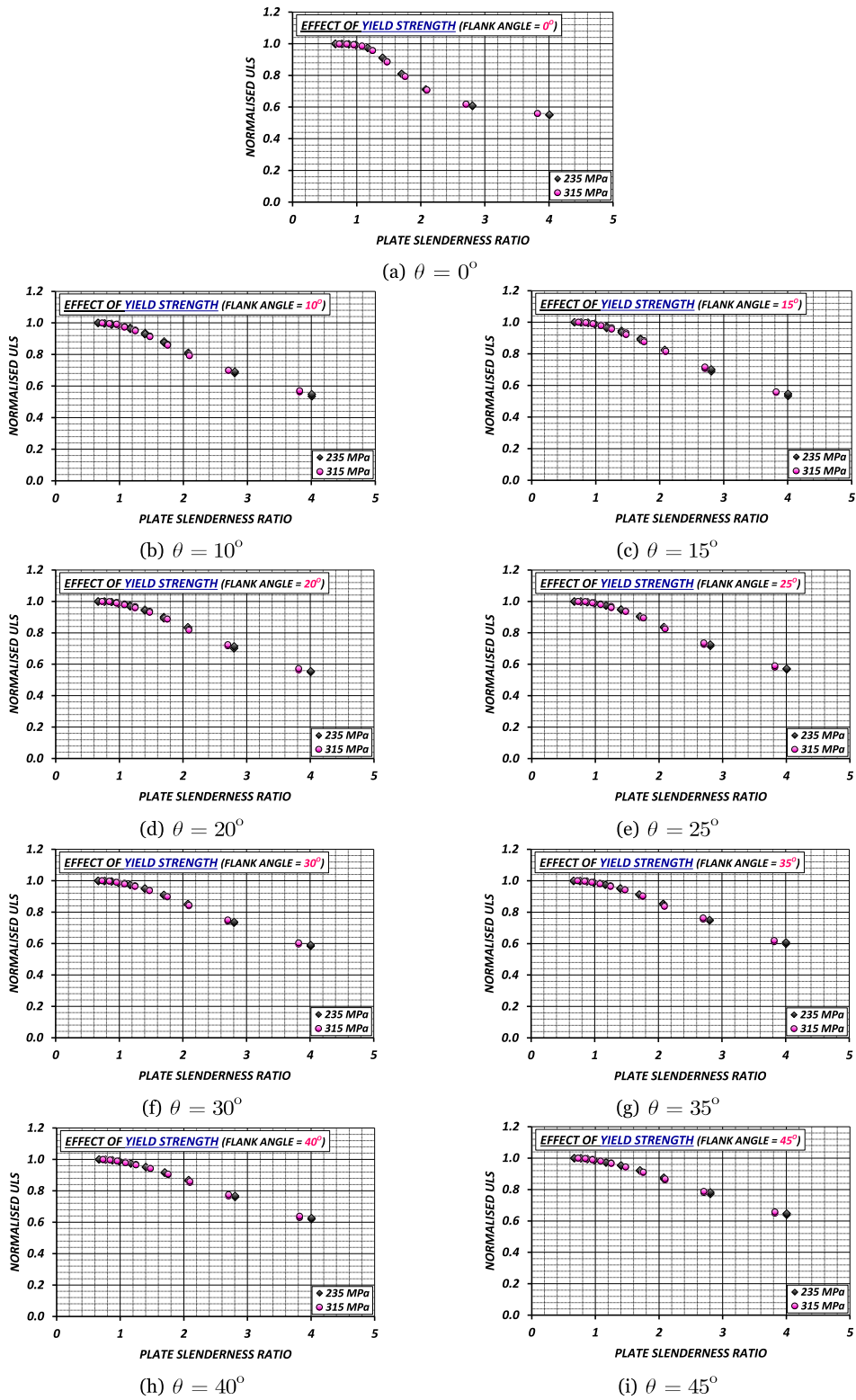Based on the outcomes mentioned above, we start to check the

(a) $\theta = 0^{\mathrm{o}}$

(b) $\theta = 10^{\mathrm{o}}$

(c) $\theta = 15^{\mathrm{o}}$

(d) $\theta = 20^{\mathrm{o}}$

(e) $\theta = 25^{\mathrm{o}}$

(f) $\theta = 30^{\mathrm{o}}$

(g) $\theta = 35^{\mathrm{o}}$

(h) $\theta = 40^{\mathrm{o}}$

(i) $\theta = 45^{\mathrm{o}}$

Fig. 12. Effect of material yield strength on the ultimate strength performance.
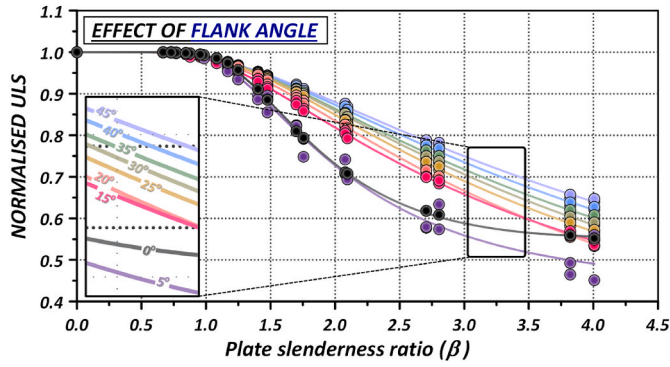
Fig. 13. Effect of the flank angle on the ultimate strength performance.

applicability of Eq. (9) by calculating the coefficient of determination (R^2). As a first step, several 2D diagrams are plotted based on the selected flank angles, which means that all scenarios within the same flank angle are plotted together in Fig. 14(a)–(j) by neglecting the effect of plate aspect ratio and material yield strength. In addition, we assumed that the normalised ULS ($=\sigma_{xu}/\sigma_Y$) predicted by formulation starts from 1.0, which means that the ultimate strength should not exceed the material yield strength. This can be expressed by the point information (x, y) in the 2D diagram. For the determination of sub-coefficients (f_1 to f_4), we added the initial point at (0, 1) in the 2D graphs shown in Fig. 14(a)-(j).

As would be expected, the general shape of the empirical formulation in Eq. (9) is applicable in predicting the ULS of the curved plate with good agreements ($R^2 = 0.988$ to 0.999). In particular, FE results were well-fitted with the empirical formulation in most flank angle cases ($10^o \leq \theta \leq 45^o$ and $\theta = 0$). In contrast, the fluctuation behaviour of ULS causes a relatively lower $R^2(= 0.9875)$ value in $\theta = 5^o$. However, it is believed that the proposed design formula could be applicable enough to estimate the ULS of the curved plate ($\beta \leq 3.0$).

As summarised in Fig. 14(a)-(j), individual sub-coefficients (f_1 to f_4) for selected flank angle scenarios are being extracted from the regression. On the other hand, there is a limitation in Fig. 14 results where it cannot predict the ULS for other flank angle cases, i.e., $\theta = 3^o, 14^o, 23^o$,

$32^o, 43^o$ or others. Therefore, further processing is needed to establish the relationship between sub-coefficients (f_1 to f_4) and flank angle (θ). As a first step, a 2D diagram plots as the flank angle increases in Fig. 15 to identify the trend of the four (4) sub-coefficients (f_1 to f_4).

The trendlines expressed in Fig. 15 by the higher-order polynomial function show good agreement with extracted data ($R^2 \simeq 0.9848$ to 0.9971). Data scientists define that fitting can be categorised into three types: overfitting, optimum, and underfitting, as presented in Fig. 16. The obtained fitting curves, which represent the relationship between sub-coefficients (f_1 to f_4) and flank angle (θ), can be considered as optimum results based on the expression in Fig. 16.

However, we should remember that all the values plotted in Fig. 15 reveal individual ULS and plate slenderness ratio curves. It means that we would better find between overfitting and optimum results from the expression in Fig. 16 by attempting to find a relevant condition that passes through those points but is not overfitted. From the investigation in Fig. 15, trend lines tend to decay when the flank angle exceeds 10°. This also matches our assumption and observation about the ULS behaviour with small flank angles, as discussed in section 4.2. From this, we found that the quadratic or tertiary polynomial is appropriate by showing nearly 1.0 of R^2. Similarly, the flank angle is divided into three ranges, as illustrated in Eq. (10).

$$f_{i=1\ to\ 4} = A_1\theta^3 + A_2\,\theta^2 + A_3\,\theta + A_4$$

$$where, A_{i=1\ to\ 4}\ will\ be\ decided\ based\ on\ three\ range \begin{cases} 0 \leq \theta \leq 10 \\ 10 < \theta \leq 30 \\ 30 < \theta \leq 45 \end{cases}$$

$$(Eq.\ 10)$$

Besides, we found out that f_3 is not significantly affected by the changes in the flank angle. Therefore, we decided to use the mean value of f_3 ($= -2.8068 \times 10^{-7}$), which is nearly zero. Finally, the developed empirical formulation summarised in Eq. (11) can predict the cylindrically curved plate's ultimate strength performance in longitudinal compression by adopting the varying effect of the flank angle ($0 \leq \theta \leq 45$).

4.3.1. Proposed empirical formulation

The proposed empirical formulation and detailed coefficients determined from a/b = 2 and 5 cases are summarised in Eq. (11).

$$\frac{\sigma_{xu}}{\sigma_Y} = 1 - \exp\left(\frac{f_1}{\beta} + \frac{f_2}{\beta^2} + \frac{f_3}{\beta^3} + f_4\right)$$

$$where, f_1\ to\ f_4 = f(\theta) = A_1\theta^3 + A_2\theta^2 + A_3\theta + A_4; \quad (Eq.\ 11)$$

$$\beta = plate\ slenderness\ ratio = \frac{b}{t}\sqrt{\frac{\sigma_Y}{E}};$$

$$\theta = flank\ angle.$$

Sub-coefficients	Flank angle range	A_1	A_2	A_3	A_4
f_1	$0 \leq \theta \leq 10$	–	−0.02978	−0.24789	2.98313
	$10 < \theta \leq 30$	−0.00073	0.04484	−0.90218	2.79235
	$30 < \theta \leq 45$	0.00091	−0.10295	3.80425	−49.50583
f_2	$0 \leq \theta \leq 10$	–	0.02177	0.28736	−6.64353
	$10 < \theta \leq 30$	0.00055	−0.03207	0.59304	−4.87304
	$30 < \theta \leq 45$	−0.00087	0.09901	−3.64250	42.70575
f_3	$0 \leq \theta \leq 10$				-2.8068×10^{-7}
	$10 < \theta \leq 30$				
	$30 < \theta \leq 45$				
f_4	$0 \leq \theta \leq 10$	–	0.00106	0.09659	−1.14350
	$10 < \theta \leq 30$	0.00018	−0.01136	0.23082	−1.42162
	$30 < \theta \leq 45$	−0.00016	0.01855	−0.69214	8.57414

*Note: f3 is a relatively small value, and may not significantly affect the ULS results.
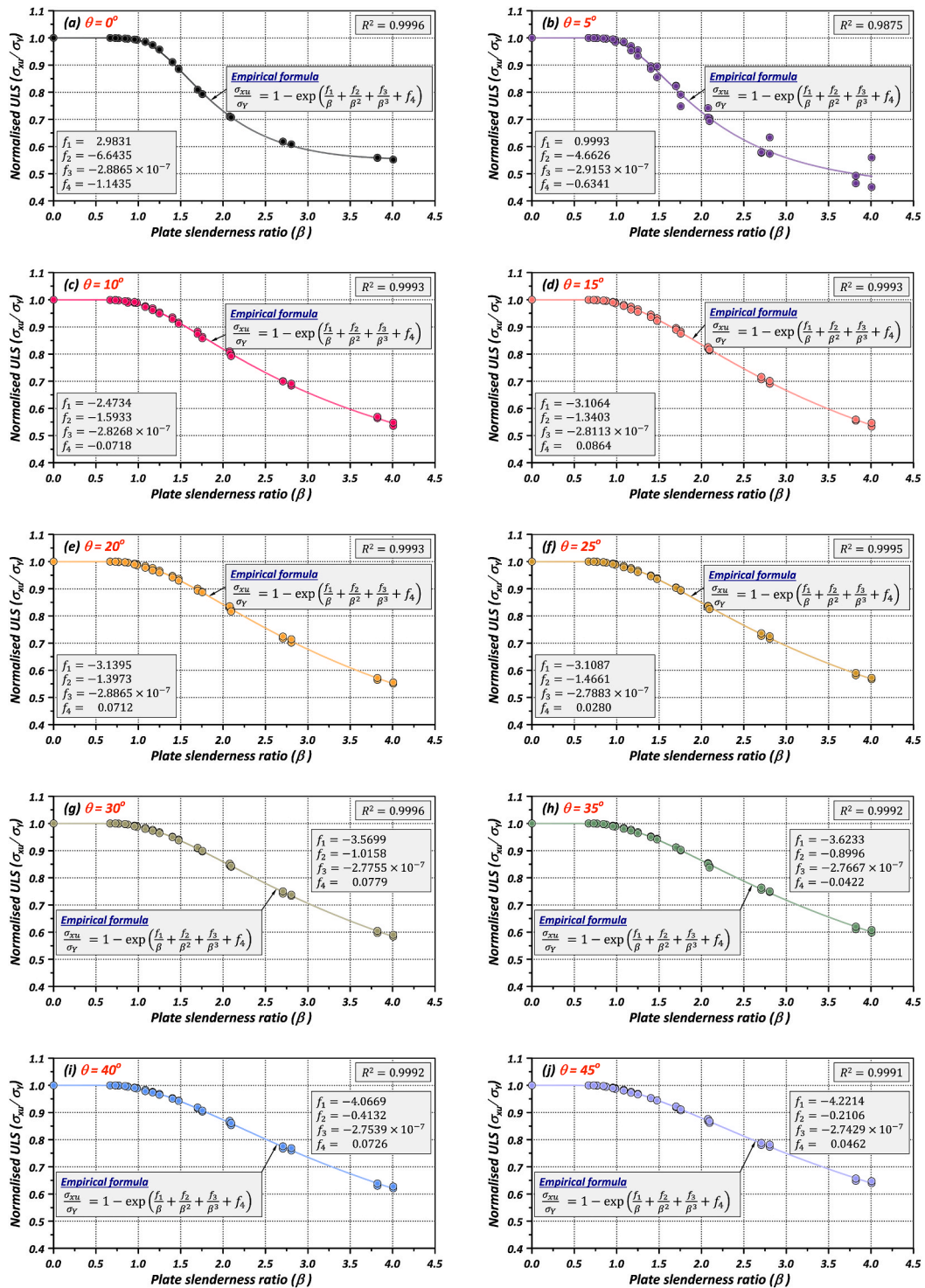
Fig. 14. Empirical formulations for each flank angle by determination of sub-coefficients using the curve-fitting method.
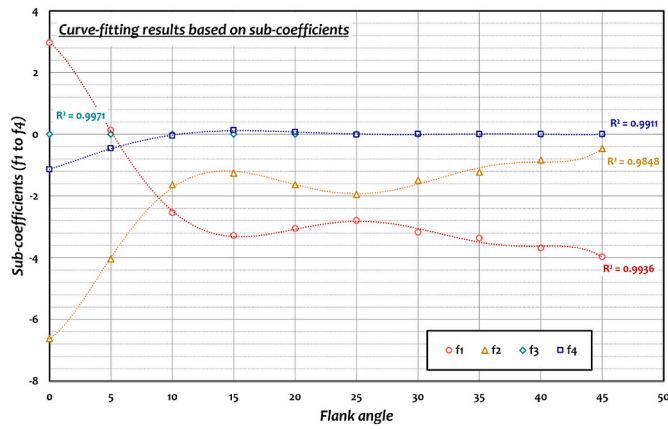
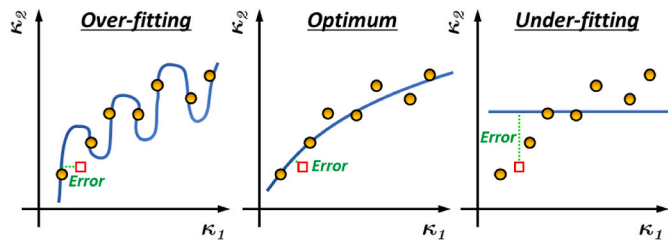**Fig. 15.** Determination of sub-coefficients by curve-fitting method.

Fig. 16. Types of fittings in predicting the data trend (Sharama, 2017).

Table 2
Additionally, selected scenarios for the validation of the proposed empirical formulation.

Comparison scenario	a (mm)	b (mm)	t (mm)	θ (deg.)	σ_Y (MPa)	E (MPa)	β
No. 1 (Fig. 17)	800	400	6.0	2.86	343	210,000	2.8
No. 2 (Fig. 18)			7.0	5.72			2.29
No. 3 (Fig. 19)			8.0	11.86			2.01
Total number of additional scenarios for validation with test results							
$\underset{a}{1} \times \underset{b}{1} \times \underset{t}{3} \times \underset{\theta}{3} \times \underset{\sigma_Y}{1} \times \underset{E}{1} = 9 \; scenarios$							

5. Validation of the proposed empirical formulation

Verifying the developed empirical formula is essential by comparing it with analytical or experimental study outcomes. It can also be compared with the existing empirical formulations. There are a number of existing formulations. However, we aim to verify the proposed formulation's applicability in this study with the testing results as our priority. As briefly introduced in Section 2, the ULS results were calculated by Maeno et al. (2004) and Kim et al. (2014) for the comparison.

Fortunately, Kim et al. (2021) recently conducted an experimental study to provide valuable test results. Therefore, we set additional curved plate scenarios based on testing results, as shown in Table 2. The detailed test information may be referred to Kim et al. (2021), and they have selected a/b = 1.0, 1.5 and 2.0. As shown in Table 2, only a/b = 2.0 and 5.0 cases were used to develop the empirical formulation. Therefore, the test results of a/b = 2.0 are only extracted from their study for comparison purposes.

The curved plate's ultimate strength performance under longitudinal compression is expressed by the 2D diagrams, representing the relationship between ULS and plate slenderness ratio. Three diagrams are prepared based on three flank angles, i.e., 2.86, 5.72 and 11.86, as shown in Figs. 17–19, respectively. Before validating the structural
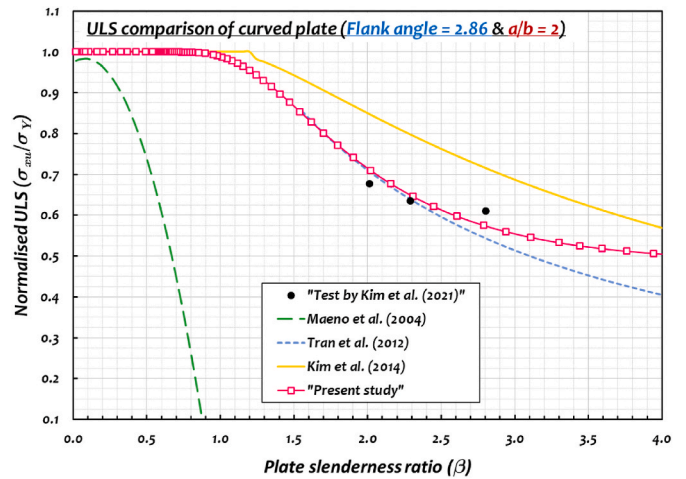

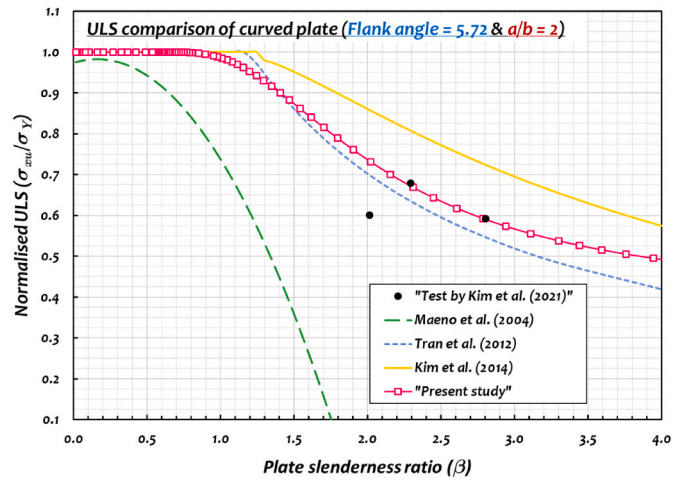**Fig. 17.** Comparison of the ULS at a flank angle (θ) of 2.86º (Scenario No. 1 in Table 2).

Fig. 18. Comparison of the ULS at a flank angle (θ) of 5.72º (Scenario No. 2 in Table 2).
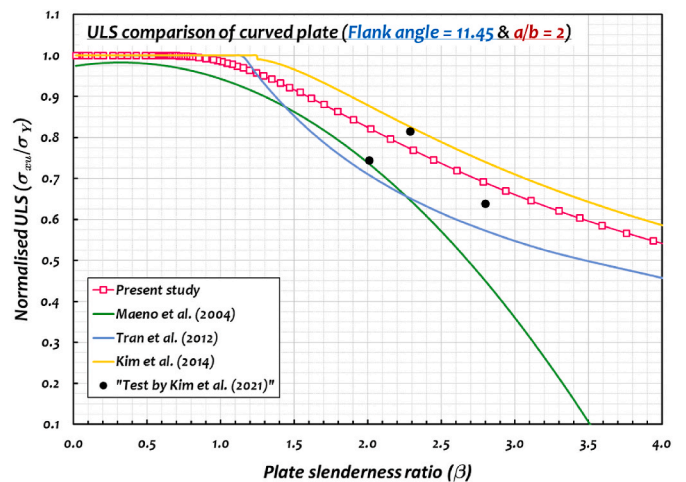

Fig. 19. Comparison of the ULS at a flank angle (θ) of 11.45º (Scenario No. 3 in Table 2).

behaviour, we should remind that the test results by Kim et al. (2021) only focus on the small flank angle range. It means that each formula has a different background and assumption. Therefore, underrating the validation results, which are not well-fitted with test results, is not recommended.

Fig. 17 shows three empirical formulations about $\theta = 2.86$, proposed by Maeno et al. (2004), Kim et al. (2014) and the formula by the present study, compared with the test results. As would be expected, we confirmed that the ULS tends to decrease as plate slenderness increased from the test and empirical formulations in the selected β range (=2.0 to 2.8). In general, the test results were well-fitted with the proposed formula.

Continuously, $\theta = 5.72$ results are plotted in Fig. 17(b). A similar trend was observed except for $\beta = 2.01$ case, which shows a lower ULS than expected. It may be expressed for the following reasons.

- **[Reason 1]** Complex geometric behaviour varying with small flank angles
- **[Reason 2]** Effect of initial deflection shape

Regarding 1st Park et al. (2018) and Kim et al. (2021) clearly stated that secondary buckling could cause a significant decrease in ULS due to the change in buckling mode shape. In addition, this behaviour can easily be captured under specific conditions, as shown in Fig. A1 provided by Park et al. (2018). They also investigated the changes in the in-plane stress distribution due to large deflection and the snap-back phenomenon that contributes to showing secondary buckling behaviour in the specific slenderness ratio and small flank angle with a particular aspect ratio.

In the case of the 2nd reason, it is reported that the different initial deflection modes may affect the ultimate strength behaviour. Besides, the initial deflection amount contributes to ULS behaviour, as shown in Fig. A2. Kim et al. (2021) stated that they did not measure the mode type and amount of the initial deflection, but this may be one of the reasons to be placing a lower ULS value at $\beta = 2.01$ than other cases ($\beta = 2.29$ and 2.8) shown in Fig. 18.

A similar trend is observed in scenario No. 3 ($\theta = 11.45°$), as shown in Fig. 19. The test results tend to fluctuate more than other cases shown in Figs. 17 and 18. However, we could confirm that the proposed empirical formula practically applies to predicting the curved plate's ultimate strength from the comparison plots presented in Figs. 17–19.

From the comparison of the ULS in Figs. 17–19, we compared how the other formulas behave in predicting the ULS of the curved plate. However, the background to develop each formula and assumed conditions are not precisely the same. Therefore, it would be better not to evaluate the accuracy of each formula.

6. Application of obtained outcome

6.1. Use of developed empirical formula

A simplified and practical empirical formula was developed based on the research procedure in Fig. 2. Also, its applicability was validated by comparison with testing and other existing formulas in section 5. A useful user guide is documented in this section by providing an example for a better understanding and practical use of the proposed empirical formula.

Fig. 20 shows the procedure to utilise the empirical formula with a detailed explanation. An example may help potential readers, i.e., students, lecturers, engineers, structural designers, etc., to calculate the
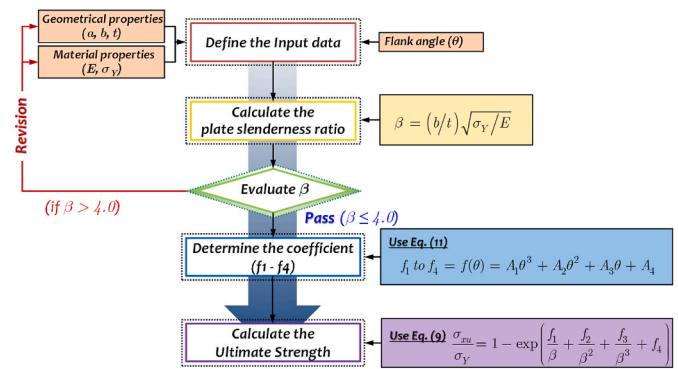

Fig. 20. Guide for a developed empirical formula to calculate the ultimate strength of the curved plate.
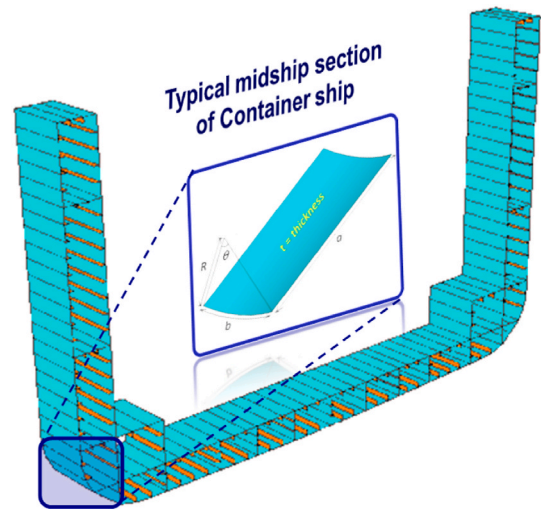

Fig. 21. Example of the cylindrically curved plate from the mid-ship section of a container ship.

ULS assessment of curved plates under longitudinal compression (see Fig. 21 and section 6.2).

6.2. Example (tutorial)

(Question) A cylindrically curved plate ($a \times b \times t = 4000mm \times 800mm \times 20mm$) from Fig. 21 with 20° of flank angle is set as a target structure that used HT32 ($E = 205.8GPa$ & $\sigma_Y = 315MPa$). If the applied longitudinal compression is 200 MPa from the extreme hogging bending moment, assess the safety based on the ultimate limit state (ULS).

(Note: lateral pressure effect can be neglected. In addition, all values used in this example are assumed and unrelated to the actual scantling).

(Solution)

[Step 1]. Define the input data

● Material properties

$\sigma_Y = 315$ MPa, $E = 205,800$ MPa

● Geometric properties

$a = 4000$ mm, $b = 800$ mm, $t = 20$ mm

[Step 2]. Calculate the plate slenderness ratio

$$\beta = \frac{b}{t}\sqrt{\frac{\sigma_Y}{E}} = \frac{800}{20}\sqrt{\frac{315}{205800}} = 1.564921593$$

$$\therefore \beta \simeq \underline{1.5649}$$

[Step 3]. Evaluate the plate slenderness ratio

There should be no limitation on the plate slenderness ratio. However, the proposed empirical formula is obtained by the assumed scenario, which ranges $0.67 \leq \beta \leq 4.01$. Therefore, it is recommended to limit β not to exceed 4.0.

$$\beta = \underline{1.5649} \leq 4.0 \therefore \underline{OK!}$$

[Step 4]. Determine the coefficient (f_1 to f_4)

You can determine the four coefficients (f_1 to f_4) by following the equation summarised in Eq. (11).

$$f_1 \text{ to } f_4 = f(\theta) = A_1\theta^3 + A_2\theta^2 + A_3\theta + A_4;$$

However, 20° of flank angle cases were directly given in Fig. 14(e). Therefore, the following coefficients are determined. If the required flank angle is not given in Fig. 14, coefficients can be calculated by Eq. (11) in Eq. (11).

$$f_1 = -3.1395 ;$$
$$f_2 = -1.3973 ;$$
$$f_3 = -2.8865 \times 10^{-7} ;$$
$$f_4 = 0.0712$$

[Step 5]. Calculate the ultimate strength of the curved plate in longitudinal compression

$$\frac{\sigma_{xu}}{\sigma_Y} = 1 - \exp\left(\frac{f_1}{\beta} + \frac{f_2}{\beta^2} + \frac{f_3}{\beta^3} + f_4\right)$$

$$= 1 - \exp\left(-\frac{3.1395}{1.5649} - \frac{1.3973}{1.5649^2} - \frac{2.8865 \times 10^{-7}}{1.5649^3} + 0.0712\right)$$

$$= 0.918372 \simeq \underline{0.9183}$$

$$\therefore \sigma_{xu} = 0.9183 \times \sigma_Y = 0.9183 \times 315 \simeq 289.3 \; \underline{MPa}$$

[Step 6]. Safety assessment based on ULS

$$Demand \, (= 200 \, MPa) < Capacity \, (= 289.3 \, MPa)$$

$$or \; Safety \; Factor = \frac{Capacity}{Demand} = 1.4465 > 1.0$$

$$\therefore \underline{Safe}!$$

A simple example was covered in this section, and it may help better understand how to utilise the developed empirical formula.

7. Conclusions

This research introduced an advanced empirical formula designed to accurately predict the ultimate limit state (ULS) of cylindrically curved plates when subjected to longitudinal compression. The systematic approach to this formula's development is articulated through these stages: (a) collection of the data, (b) definition of structural characteristics (i.e., geometric and material properties), (c) selection of reliable scenarios, (d) calculation of ultimate limit state (ULS), (e) data processing, (f) development of the formula, and (g) validation.

● **Contribution No. 1: Development of the empirical formula**

The foundational structure of the proposed formula, as shown in Eq. (11a), was validated using 400 nonlinear finite element (NLFEM) simulation cases. This extensive validation allowed for the precise determination of sub-coefficients in Eq. (11b), with high R^2 values exceeding 0.99, as illustrated in Fig. 14. While the 400 curved plate scenarios addressed in this study provide a broad overview, they might not cover the entire variability of the structural behaviour. Therefore, the coefficients in Eq. (11b) may benefit from refinement by including more diverse scenarios in future research.

● **Contribution No. 2: Validation with Test results**

Furthermore, the proposed formula's performance was compared with experimental results, as presented in Figs. 17–19. The empirical formula's results aligned well with these experimental findings, confirming its relevance and effectiveness in estimating the ultimate strength of curved plates under longitudinal compression.

● **Contribution No. 3: User's guide**

To wrap up the study, a practical example, complemented by a user guide, is provided in Section 6. This inclusion aims to assist practitioners in understanding and effectively implementing the newly proposed empirical formula."

● **Limitation**

Notably, the effects of the aspect ratio and the small flank angle are areas that merit further exploration in future research endeavors.

Declaration of competing interest

The authors declare that they have no known competing financial interests or personal relationships that could have appeared to influence the work reported in this paper.
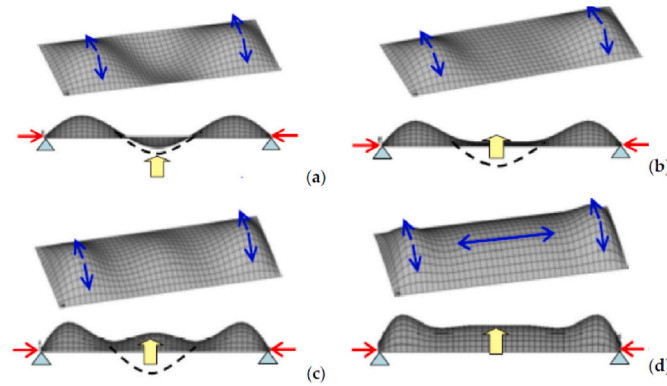
Acknowledgements

Appendix

Fig. A.1. Example of the deflection shape changes in small flank angle subjected to longitudinal compression (Park et al., 2018).
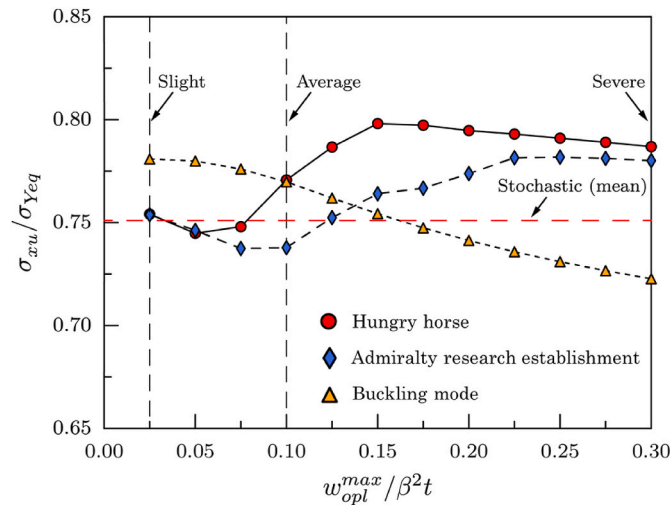

Fig. A.2. Effect of initial deflection mode shape and magnitude on the ultimate strength performance of the plate. (Georgiadis et al., 2021).

References

ANSYS, 2014. User Manual, 13 ed. ANSYS Inc., Canonsburg, PA, USA, Version 13.0.

Anyfantis, K.N., 2020. Ultimate strength of stiffened panels subjected to non-uniform thrust. Int. J. Nav. Archit. Ocean Eng. 12, 325–342.

Chen, Y., 2003. Ultimate Strength Analysis of Stiffened Panels Using a Beam-Column Method. Virginia Polytechnic Institute and State University, Blacksburg, VA, USA.

Cho, S.-R., Muttaqie, T., Do, Q.T., So, H.Y., Sohn, J.-M., 2018. Ultimate strength formulation considering failure mode interactions of ring-stiffened cylinders subjected to hydrostatic pressure. Ocean. Eng. 161, 242–256.

Cho, S.-R., Muttaqie, T., Do, Q.T., Park, S.H., Kim, S.M., So, H.Y., Sohn, J.M., 2019. Experimental study on ultimate strength of steel-welded ring-stiffened conical shell under external hydrostatic pressure. Mar. Struct. 67, 102634.

DNVGL, 2015. Buckling Class Guideline. DNVGL, Oslo, Norway.

Domb, M., Leigh, B., 2001. Refined design curves for compressive buckling of curved panels using nonlinear finite element analysis. In: 19th AIAA Applied Aerodynamics Conference. American Institute of Aeronautics and Astronautics.

Faulkner, D., 1975. A review of effective plating for use in the analysis of stiffened plating in bending and compression. J. Ship Res. 19 (1), 1–17.

Frankland, J.M., 1940. The strength of ship plating under edge compression. US Experimental Model Basin Progress Report 469.

Fujikubo, M., Yao, T., Varghese, B., 1997. Buckling and ultimate strength of plates subjected to combined loads. In: The Seventh International Offshore and Polar Engineering Conference. International Society of Offshore and Polar Engineers.

Fujikubo, M., Kaeding, P., 2002. New simplified approach to collapse analysis of stiffened plates. Mar. Struct. 15 (3), 251–283.

Georgiadis, D.G., Samuelides, M.S., Li, S., Kim, D.K., Benson, S., 2021. Influence of stochastic geometric imperfection on the ultimate strength of stiffened panel in compression. In: The 8th International Conference on Marine Structures (MARSTRUCT 2021), 7-9 June, Trondheim, Norway.

Guedes Soares, C., 1988. Design equation for the compressive strength of unstiffened plate elements with initial imperfections. J. Constr. Steel Res. 9 (4), 287–310.

ISSC, 2012. Ultimate strength (committee III.1). In: The 18th International Ship and Offshore Structures Congress (ISSC 2012), 9-13 September, Rostock, Germany.

Khedmati, M.R., Zareei, M.R., Rigo, P., 2010. Empirical formulations for estimation of ultimate strength of continuous stiffened aluminium plates under combined in-plane compression and lateral pressure. Thin-Walled Struct. 48 (3), 274–289.

Kim, D.K., Park, D.H., Kim, H.B., Kim, B.J., Seo, J.K., Paik, J.K., 2013a. Lateral pressure effects on the progressive hull collapse behaviour of a Suezmax-class tanker under vertical bending moments. Ocean. Eng. 63, 112–121.

Kim, D.K., Pedersen, P.T., Paik, J.K., Kim, H.B., Zhang, X., Kim, M.S., 2013b. Safety guidelines of ultimate hull girder strength for grounded container ships. Saf. Sci. 59, 46–54.

Kim, D.K., Lim, H.L., Kim, M.S., Hwang, O.J., Park, K.S., 2017. An empirical formulation for predicting the ultimate strength of stiffened panels subjected to longitudinal compression. Ocean. Eng. 140, 270–280.

Kim, D.K., Lim, H.L., Yu, S.Y., 2018a. A technical review on ultimate strength prediction of stiffened panels in axial compression. Ocean. Eng. 170, 392–406.

Kim, D.K., Poh, B.Y., Lee, J.R., Paik, J.K., 2018b. Ultimate strength of initially deflected plate under longitudinal compression: Part I = an advanced empirical formulation. Struct. Eng. Mech. 68 (2), 247–259.

Kim, D.K., Lim, H.L., Yu, S.Y., 2019. Ultimate strength prediction of T-bar stiffened panel under longitudinal compression by data processing: a refined empirical formulation. Ocean. Eng. 192, 106522.

Kim, D.K., Kim, H.B., Park, D.H., Mohd, H.M., Paik, J.K., 2020a. A practical diagram to determine the residual longitudinal strength of grounded ship in Northern Sea Route. Ships Offshore Struct. 15 (7), 683–700.

Kim, D.K., Yu, S.Y., Lim, H.L., Cho, N.-K., 2020b. Ultimate compressive strength of stiffened panel: an empirical formulation for flat-bar type. J. Mar. Sci. Eng. 8 (8), 605.

Kim, D.K., Li, S., Lee, J.R., Poh, B.Y., Benson, S., Cho, N.-K., 2022a. An empirical formula to assess ultimate strength of initially deflected plate: Part 1 = propose the general shape and application to longitudinal compression. Ocean. Eng. 252, 111151.

Kim, D.K., Li, S., Yoo, K., Danasakaran, K., Cho, N.-K., 2022b. An empirical formula to assess ultimate strength of initially deflected plate: Part 2 = combined longitudinal compression and lateral pressure. Ocean. Eng. 252, 111112.

Kim, D.K., Ban, I., Poh, B.Y., Shin, S.-C., 2023. A useful guide of effective mesh-size decision in predicting the ultimate strength of flat- and curved plates in compression. J. Ocean Eng. Sci. 8 (4), 401–417.

Kim, J.-H., Park, D.-H., Kim, S.-K., Kim, M.-S., Lee, J.-M., 2021. Experimental study and development of design formula for estimating the ultimate strength of curved plates. Appl. Sci. 11 (5).

Kim, J.H., Park, J.S., Lee, K.H., Kim, J.H., Kim, M.H., Lee, J.M., 2014. Computational analysis and design formula development for the design of curved plates for ships and offshore structures. Struct. Eng. Mech. 49 (6), 705–726.

Li, S., Kim, D.K., Benson, S., 2021. The influence of residual stress on the ultimate strength of longitudinally compressed stiffened panels. Ocean. Eng. 231, 108839.

Li, S., Kim, D.K., 2022. Ultimate strength characteristics of unstiffened cylindrical shell in axial compression. Ocean. Eng. 243, 110253.

Li, S., Kim, D.K., Liang, Q.Q., 2022. Fibre-Based modelling for predicting the progressive collapse of cylindrical shells under combined axial compression and bending moment. Eng. Struct. 272, 114988.

Lin, Y.-T., 1985. Ship Longitudinal Strength Modelling. Ph.D. Dissertation, Department of Naval Architecture and Ocean Engineering, University of Glasgow, Scotland, UK.

Liu, B., Gao, L., Ao, L., Wu, W., 2021. Experimental and numerical analysis of ultimate compressive strength of stiffened panel with openings. Ocean. Eng. 220, 108453.

Maeno, Y., Yamaguchi, H., Fujii, Y., Yao, T., 2004. Buckling/plastic collapse behaviour and strength of bilge circle and its contribution to ultimate longitudinal strength of Ship¿s hull girder. In: The 14th International Offshore and Polar Engineering Conference (ISOPE 2014). ISOPE, Toulon, France, pp. 296–302.

Martins, J.P., Simões da Silva, L., Reis, A., 2013. Eigenvalue analysis of cylindrically curved panels under compressive stresses – extension of rules from EN 1993-1-5. Thin-Walled Struct. 68, 183–194.

Martins, J.P., Simões da Silva, L., Reis, A., 2014. Ultimate load of cylindrically curved panels under in-plane compression and bending—extension of rules from EN 1993-1-5. Thin-Walled Struct. 77, 36–47.

Martins, J.P., Beg, D., Sinur, F., Simões da Silva, L., Reis, A., 2015. Imperfection sensitivity of cylindrically curved steel panels. Thin-Walled Struct. 89, 101–115.

Martins, J.P., Simões da Silva, L., Silvestre, N., 2016. Energy-based analytical model to predict the elastic critical behaviour of curved panels. J. Constr. Steel Res. 127, 165–175.

Martins, J.P., Ljubinkovic, F., Simões da Silva, L., Gervásio, H., 2018. Behaviour of thin-walled curved steel plates under generalised in-plane stresses: a review. J. Constr. Steel Res. 140, 191–207.

Paik, J.K., Thayamballi, A.K., 1997. An empirical formulation for predicting the ultimate compressive strength of stiffened panels. In: The 7th International Offshore and Polar Engineering Conference, ISOPE-I-97-444. ISOPE 1997), 25-30 May, Honolulu, Hawaii, USA.

Paik, J.K., Thayamballi, A.K., Lee, J.M., 2004. Effect of initial deflection shape on the ultimate strength behavior of welded steel plates under biaxial compressive loads. J. Ship Res. 48 (1), 45–60.

Paik, J.K., 2007. Empirical formulations for predicting the ultimate compressive strength of welded aluminum stiffened panels. Thin-Walled Struct. 45 (2), 171–184.

Paik, J.K., Kim, D.K., Lee, H., Shim, Y.L., 2012a. A method for analyzing elastic large deflection behavior of perfect and imperfect plates with partially rotation-restrained edges. J. Offshore Mech. Arctic Eng. 134 (2), 021603.

Paik, J.K., Kim, D.K., Park, D.H., Kim, H.B., Kim, M.S., 2012b. A new method for assessing the safety of ships damaged by grounding. International Journal of Maritime Engineering 154 (Part A1), 1–20.

Paik, J.K., 2018a. Ultimate Limit State Analysis and Design of Plated Structures, second ed. John Wiley & Sons, Chichester, UK.

Paik, J.K., 2018b. Ultimate Limit State Analysis and Design of Plated Structures. John Wiley & Sons, Chichester, UK.

Paik, J.K., 2020. Advanced Structural Safety Studies: with Extreme Conditions and Accidents. Springer Singapore, Singapore.

Park, J.-S., Fujikubo, M., Iijima, K., Yao, T., 2009. Prediction of the secondary buckling strength and ultimate strength of cylindrically curved plate under axial compression. In: The Nineteenth International Offshore and Polar Engineering Conference.

Park, J.-S., Iijima, K., Yao, T., 2011. Buckling/ultimate strength and progressive collapse behaviour comparison of unstiffened and stiffened curved plates subjected to axial compression. Int. J. Comput. Appl. Technol. 41 (1–2), 60–72.

Park, J.S., Paik, J.K., Seo, J.K., 2018. Numerical investigation and development of design formula for cylindrically curved plates on ships and offshore structures. Thin-Walled Struct. 132, 93–110.

Seo, J.K., Song, C.H., Park, J.S., Paik, J.K., 2016. Nonlinear structural behaviour and design formulae for calculating the ultimate strength of stiffened curved plates under axial compression. Thin-Walled Struct. 107, 1–17.

Sharama, S., 2017. Epoch vs Batch Size vs Iterations (Link. https://towardsdatascience.com/epoch-vs-iterations-vs-batch-size-4dfb9c7ce9c9). Medium, pp. https://towardsdatascience.com/epoch-vs-iterations-vs-batch-size-4dfb9c7ce9c9.

Smith, C.S., Davidson, P.C., Chapman, J.C., Dowling, P.J., 1988. Strength and Stiffness of Ships'plating under In-Plane Compression and Tension, vol. 130. Royal Institution of Naval Architects Transactions, pp. 277–296.

Tanaka, Y., Endo, H., 1988. Ultimate strength of stiffened plates with their stiffeners locally buckled in compression. J. Soc. Nav. Archit. Jpn. 1988 (164), 456–467.

Tran, K.L., Davaine, L., Douthe, C., Sab, K., 2012. Stability of curved panels under uniform axial compression. J. Constr. Steel Res. 69 (1), 30–38.

Tran, K.L., Douthe, C., Sab, K., Dallot, J., Davaine, L., 2014. Buckling of stiffened curved panels under uniform axial compression. J. Constr. Steel Res. 103, 140–147.

Ueda, Y., Yasukawa, W., Yao, T., Ikegami, H., Ominami, R., 1975. Ultimate strength of square plates subjected to compression (1st Report). J. Soc. Nav. Archit. Jpn. 1975 (137), 210–221.

Ueda, Y., Yao, T., Nakacho, K., Yuan, M.G., 1992. Prediction of welding residual stress, deformation and ultimate strength of plate panels. Trans. JWRI 21 (2), 137–143.

Wong, A.M.K., 2019. An Empirical Formulation for Predicting the Ultimate Strength of Unstiffened Curved Plates Subjected to Longitudinal Compression (BEng. Dissertation). Department of Civil and Environmental Engineering. PETRONAS University of Technology, Seri Iskandar, Malaysia.

Xu, G., Qin, K., Yan, R., Dong, Q., 2022. Research on failure modes and ultimate strength behavior of typical sandwich composite joints for ship structures. Int. J. Nav. Archit. Ocean Eng. 14, 100428.

Xu, M.C., Song, Z.J., Zhang, B.W., Pan, J., 2018. Empirical formula for predicting ultimate strength of stiffened panel of ship structure under combined longitudinal compression and lateral loads. Ocean. Eng. 162, 161–175.

Youssef, S.A.M., Faisal, M., Seo, J.K., Kim, B.J., Ha, Y.C., Kim, D.K., Paik, J.K., Cheng, F., Kim, M.S., 2016. Assessing the risk of ship hull collapse due to collision. Ships Offshore Struct. 11 (4), 335–350.

Zhang, S., Khan, I., 2009. Buckling and ultimate capability of plates and stiffened panels in axial compression. Mar. Struct. 22 (4), 791–808.